IEEE Access
Multidisciplinary | Rapid Review | Open Access Journal

SPECIAL SECTION ON COLLABORATION FOR INTERNET OF THINGS

Received December 10, 2018, accepted December 24, 2018, date of publication January 11, 2019, date of current version February 4, 2019.

Digital Object Identifier 10.1109/ACCESS.2019.2892188

EEG Processing in Internet of Medical Things Using Non-Harmonic Analysis: Application and Evolution for SSVEP Responses

DONGBAO JIA[1,2], HONGWEI DAI[1], YUTA TAKASHIMA[2], TAKURO NISHIO[2], KANNA HIROBAYASHI[2], MASAYA HASEGAWA[2], SHIGEKI HIROBAYASHI[2], (Member, IEEE), AND TADANOBU MISAWA[2]

[1]School of Computer Engineering, Huaihai Institute of Technology, Lianyungang 222005, China
[2]Graduate School of Science and Engineering, University of Toyama, Toyama 930-8555, Japan

Corresponding author: Shigeki Hirobayashi (hirobays@eng.u-toyama.ac.jp)

This work was supported in part by the JSPS KAKENHI under Grant 15H00779 and Grant 18H03259, and in part by the National Natural Science Foundation of China under Grant 61873105.

ABSTRACT In recent years, the Internet of Things has been applied in many fields with rapid development, such as software, sensors, and medical and healthcare. In the case of medical and healthcare, extensive research has focused on the development of brain–computer interface systems, particularly those utilizing steady-state visual-evoked potentials (SSVEPs). However, the conventional short-time Fourier transform (STFT) analysis is associated with the low-frequency resolution because of the length of the analysis window, resulting in sidelobe artifacts. In this paper, we utilized the non-harmonic analysis (NHA), which does not depend on the length of the analysis window, to analyze the continuous changes in and determine the classification accuracy of SSVEPs. Moreover, our experiments utilized the gray-scale images, allowing for the presentation of the stimulus as a sinusoidal pattern and reducing the effect of frequency distortion associated with the refresh rate of the liquid-crystal display. Our findings indicated that NHA resulted in exponential improvements in time–frequency resolution when compared with the STFT analysis. As the accuracy of NHA was high, our results suggest that this method is effective for examining SSVEPs and changes in brain waves during experiments conducted using liquid-crystal displays.

INDEX TERMS Brain computer interface, chirp stimulus, grayscale images, non-harmonic analysis, steady-state visual evoked potential.

I. INTRODUCTION

The Internet of things (IoT) is the network of devices, vehicles, home appliances and many other applications [1]–[3], which is an important part of the new generation of information technology, but also an important stage of development in the ''information'' era.

Based on the recognition, pervasive computing, and other communication perception technologies, the extensive applications for IoT has now covered many fields that contain software [4], sensors [5], and medical and healthcare [6], etc.

In recent years, extensive research has focused on the medical and health such as deep neural network or neuroscience related purposes, data collection and accurate analysis, then monitoring and connecting available medical resources and healthcare services [7].

Brain–computer interface (BCI) systems [8]–[10] have recently been applied to video games, service robots, and household electrical appliances [11], which utilize a computer to provide an interface between a human user and an external processing unit [12]. Many BCI systems rely on quantitative features, such as the P300—a type of event-related potential (ERP) that is time-locked to a sensory, motor, or cognitive event—or steady-state visual-evoked potentials (SSVEPs), which represent natural responses to visual stimuli presented at certain frequencies [13].

Several studies have aimed to improve the precision of BCIs [14], [15]. As the classification accuracy of SSVEP-based responses is high relative to that observed for auditory steady-state responses or other ERPs, many research groups have begun to apply SSVEPs to BCI systems [16].

However, the stimulation required to elicit SSVEPs causes marked fatigue in observers, making it difficult to conduct lengthy experiments. Research has indicated that the fatigue caused by visual stimulation is associated with the strength of the SSVEP. Stimuli presented at a frequency of approximately 10 Hz induce a high degree of fatigue, and the fatigue level increases in addition to decreases in the SSVEP amplitude in the high-frequency band [17]. Moreover, the high-frequency visual stimuli required in such settings may induce epileptic seizures, degradation of signal quality, and deterioration of system performance [18]–[21]. In addition, as the number of commands increases, it becomes increasingly important to distinguish the targets from stimuli of various frequencies, as well as to reduce the effect of the stimulus in specific frequency bands to attenuate fatigue and seizure risk [22]. Evidence suggests that frequency modulation reduces flicker perceptibility associated with SSVEP-based BCI systems, leading to improvements in user experience and performance [23].

The processing of synchronous information is essential during general SSVEP measurement [23], [24] in order to reduce noise associated with bodily movement, particularly when responses are relatively less robust or low in amplitude. Although the signal-to-noise ratio has increased, to reveal the SSVEP response induced by the stimulus frequency, it is necessary to accurately determine the time-frequency variations in the measurement response [25]. However, the accurate analysis of responses—having a variety of frequency variations and containing noise—is difficult.

The short-time Fourier transform (STFT) is widely used in the field of time-frequency analysis [26], [27], which divides a long signal into shorter segments of equal length and then computes the Fourier transform separately on each shorter segment. However, it is difficult to achieve compatibility between the time and frequency resolutions because the frequency resolution depends on the length of the analysis window. Briefly, if the window is short, the frequency resolution decreases, whereas the time resolution decreases in the case of a long window.

In contrast, non-harmonic analysis (NHA) has considerable potential in SSVEP analysis. The effectiveness of NHA has been validated for use in auditory [28], imagery [29], [30], and visual applications [31], as well as in applications associated with stock-price fluctuation [32], gravitational waves visualization [33], [34], and medical tomography technology [35]–[37]. As NHA uses the least squares method, the frequency and other associated parameters can be accurately estimated with little influence of the analysis window length; in addition, the frequency resolution remains high and even sharp changes can be correctly analyzed using a short analysis window length. In brief, high time and frequency resolutions can be simultaneously obtained. Therefore, we hypothesized that NHA can be used to analyze continuous changes in and determine the classification accuracy of SSVEP.

In the present study, we propose and attempt the application of NHA to SSVEP analysis and compare the results obtained using STFT analysis and NHA. We demonstrate that NHA is a highly precise method, which yields marked improvements in the frequency resolution. This technique is effective for analyzing and visualizing Chirp-VEPs and changes in brain waves.

II. MATERIALS AND METHODS

A. CHIRP STIMULUS

We used the chirp stimulus for performing experiments in the present study. In general, the number of channels is limited; however, this type of a stimulus may facilitate an increase in the number of BCI commands in a high-sensitivity band. As long as the slope of the frequency change differs, the stimuli will be identified as different, even when they belong to the same limited frequency band, as shown in Figure 1.

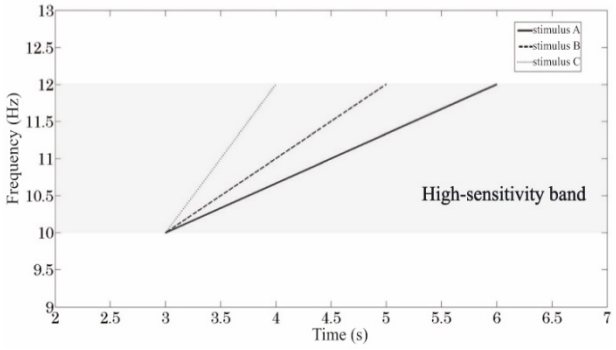

FIGURE 1. Different slopes of stimulus in the same frequency band.

SSVEP stimuli can be presented either via an LED or xenon light source [20]. When these light sources are used, the stimulus is presented directly, inducing a relatively strong response. However, external control of the device is necessary when such sources are used. Alternatively, because the size and shape can change freely using liquid crystal display (LCD), and it does not have image burn-in, LCD can display arbitrary images and the stimulus can be altered in various ways. Thus, we selected the LCD monitor to project the stimulus in the present study [38].

However, previous studies have investigated the influence of SSVEP distortion caused by the refresh rate of the monitor [39]. Although the distortion level is relatively low for the entire stimulus, high levels of distortion may occur in specific bands, and the stimulus type that can be presented depends on the refresh rate of the LCD. For example, Figure 2 depicts the waveforms obtained when only black-and-white stimuli are presented using an LCD monitor in previous studies, in which the stimulus appears as a rectangular wave, the frequency becomes discrete and distortion occurred since the frequency of the stimulus was limited to $1/N$ (N is natural number) times the refresh rate.

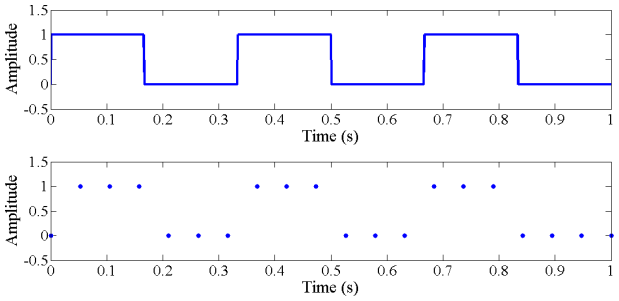

FIGURE 2. Signal of 3 Hz after sampling at 19 Hz (without grayscale image).

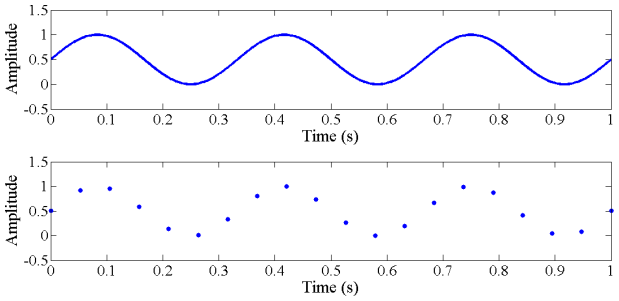

FIGURE 3. Signal of 3 Hz after sampling at 19 Hz (with grayscale image).

To reduce the distortion and limit the frequency range at which stimuli is presented, the grayscale image is added in the present study, as shown in Figure 3. Changes in the brightness value of the presented chirp stimulus occur as a sinusoidal pattern allows one to visualize frequencies that cannot be expressed using rectangular waveforms. In addition, because the distortion-induced differences in the brightness value remain close to the ideal waveform, it is possible to reduce the effect of frequency distortion associated with the refresh rate of the LCD monitor, even when the cycle has deviated.

B. ANALYSIS METHOD

The STFT as a Fourier-related transform has been commonly used for analyzing organic signals, such as the SSVEP. The Fourier transform can be represented as follows:

$$X(nf_1) = \frac{1}{T}\int_0^T x(t)e^{-j2\pi nf_1 t}dt, \tag{1}$$

where T is the analysis window length ($f_1 = 1/T$, n is a positive integer). Equation (1) is solved for determining the Fourier coefficients. As the Fourier transform is used for analyzing a completely periodic signal in an analysis window T, the calculated frequencies (nf_1) depend on the window length T, and errors frequently occur in the analysis of non-harmonic signal frequencies. Moreover, as changes in the frequency of the chirp stimulus occur sharply over a short duration, a decrease in the length of the analysis window to increase the time resolution also decreases the frequency resolution.

As the Fourier coefficient is estimated based on the least squares method, NHA [28]–[37] enables an accurate estimation of the frequency f, amplitude A, and initial phase φ, avoiding the dominance of the analysis window length. To minimize the sum of squares of the difference between the object signal and sinusoidal model signal, the f, A, and φ are calculated using the cost function, as follows:

$$F(A, f, \varphi) = \frac{1}{N}\sum_{n=0}^{N-1}\{x(n\Delta t) - A\cos(2\pi fn\Delta t + \varphi)\}^2, \tag{2}$$

where N is the total number of samples and Δt is the sampling interval ($\Delta t = 1/f_s$; here, f_s is the sampling frequency). In this way, NHA can reduce the effect of the analysis window length, and the frequency resolution remains high, enabling researchers to perform detailed analyses even when sharp changes occur within a short period of time. Therefore, in the NHA approach, a nonlinear equation is used (2) to perform the optimum calculation of the final value of f, as well as the parameters A and φ [40], [41].

By considering equation (2) as a cost function, this nonlinear optimization can be formulated as a minimization problem. In this formulation, $\hat{f}_m$ and $\hat{\varphi}_m$ are determined using the steepest descent method, producing the following expression:

$$\hat{f}_{m+1} = \hat{f}_m - \mu_m\frac{\partial F}{\partial f}, \tag{3}$$

$$\hat{\varphi}_{m+1} = \hat{\varphi}_m - \mu_m\frac{\partial F}{\partial \varphi}. \tag{4}$$

We use the following shorthand to express (3) and (4):

$$\partial F = \partial F\left(\hat{A}_m, \hat{f}_m, \hat{\varphi}_m\right). \tag{5}$$

A can be uniquely determined only if $\hat{f}_m$ and $\hat{\varphi}_m$ are known. The following formula is used to cause A to converge:

$$\hat{A}_{m+1} = \hat{A}_m - \mu_m\frac{\partial F}{\partial A}, \tag{6}$$

where μ_m is a weighting coefficient based on the retardation method and has a value between 0 and 1. This parameter is used to convert cost functions, calculated by using recurrence formulas, into a monotonically decreasing sequence [42]–[44].

This series of calculations is repeated so that $\hat{A}_m$, $\hat{f}_m$, and $\hat{\varphi}_m$ converge with high accuracy. Although the steepest descent method causes values to converge over a comparatively wide range, a single series of operations is unable to ensure sufficient accuracy. To achieve highly accurate conversion, NHA improves the accuracy by applying Newton's method after the application of the steepest descent method. The following recurrence formula is used for Newton's method:

$$\hat{f}_{m+1} = \hat{f}_m - \frac{v_m}{J}\begin{vmatrix}\frac{\partial F}{\partial f} & \frac{\partial^2 F}{\partial f\partial\varphi}\\ \frac{\partial F}{\partial \varphi} & \frac{\partial^2 F}{\partial \varphi^2}\end{vmatrix}, \tag{7}$$

$$\hat{\varphi}_{m+1} = \hat{\varphi}_m - \frac{v_m}{J}\begin{vmatrix}\frac{\partial^2 F}{\partial f^2} & \frac{\partial F}{\partial f}\\ \frac{\partial^2 F}{\partial f\partial\varphi} & \frac{\partial F}{\partial \varphi}\end{vmatrix}, \tag{8}$$

where

$$J = \begin{vmatrix} \dfrac{\partial^2 F}{\partial f^2} & \dfrac{\partial^2 F}{\partial f \partial \varphi} \\ \dfrac{\partial^2 F}{\partial f \partial \varphi} & \dfrac{\partial^2 F}{\partial \varphi^2} \end{vmatrix}. \tag{9}$$

Equations (7)-(9) can be written as

$$\partial^2 F = \partial^2 F \left(\hat{A}_m, \hat{f}_m, \hat{\varphi}_m \right), \tag{10}$$

where μ_m and v_m are weighting coefficients that are based on the retardation method [45], [46]. After applying equations (7) and (8), $\hat{A}_m$ is made to converge by applying equation (6) in the same manner as the steepest descent method and the calculation series is repeated. Thus, the frequency parameters are quickly estimated to a high degree of accuracy by using a hybrid process that combines the steepest descent method with Newton's method.

According to these analyses, the frequency value of a response fluctuates with time, a waveform having a frequency comprising integral multiples can be estimated accurately using fast Fourier transform (FFT).

However, Figure 4 shows the spectrum analysis results of a non-integer sinusoidal wave model (amplitude = 1 and frequency = 1.5) processed using the FFT (zero padding) and NHA techniques. Owing to the influence of the analysis window, when the frequency is not an integral multiple, FFT cannot splice the signal in a complete cycle, which causes the amplitude to disperse into components in adjacent frequency bands, creating a side-lobe artifact. In contrast, because the influence of the analysis window is small during NHA, side-lobe artifacts do not occur; thus, the amplitude and frequency values can be estimated accurately, even if the frequency of a particular waveform is not an integral multiple.

Therefore, NHA as a highly precise frequency analysis method can be used to examine SSVEP responses and improve the analytical precision in the present study.

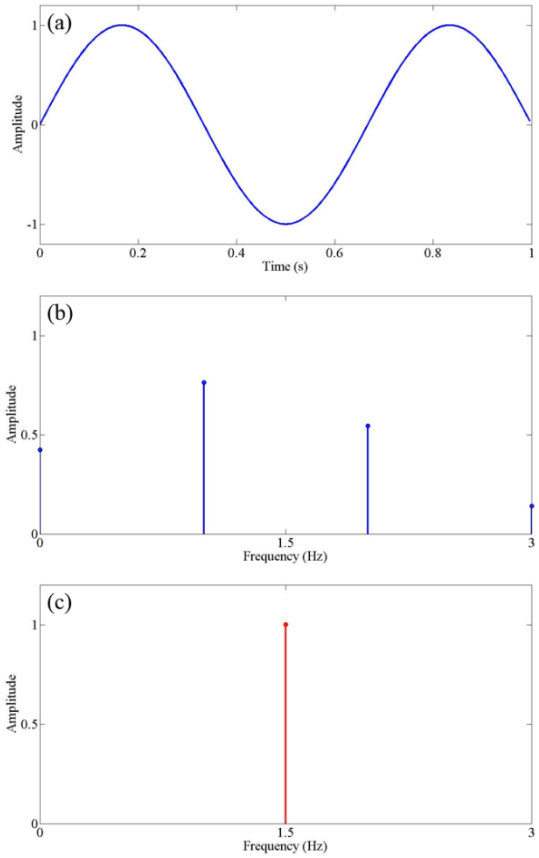

FIGURE 4. Spectrum analysis results for a non-integer waveform frequency signal with $A = 1$ and $f = 1.5$ Hz. The (a) original, (b) FFT, and (c) NHA cases are shown.

III. EXPERIMENT

A. EXPERIMENTAL ENVIRONMENT AND PARTICIPANTS

Thirty-eight-channel electroencephalography (EEG) (EMC NVX 52) was used to measure brain activity, while the participants viewed the stimulus video. Electrode placement was based on the International 10-10 system for EEG, and the A1 and A2 electrodes were used as the reference. Data were sampled at a rate of 2,000 Hz, band-pass filtered at 0.1-70 Hz, and notch filtered at 60 Hz. Stimuli were presented on a 31.5'' LCD monitor (EV3237, EIZO), which had a refresh rate of 120 Hz and was capable of a 4-K resolution.

Ten male students in their 20s with normal vision and no epilepsy history participated in the present study. All participants provided written consent to participate, and ethical approval was obtained from the institutional ethics committee [47]. Participants were positioned as shown in Figure 5. The LCD on which the stimulus was projected was placed in front of the participant at a distance of 0.6 m (presentation range: 0.33 × 0.33 m). To avoid the influence of outside

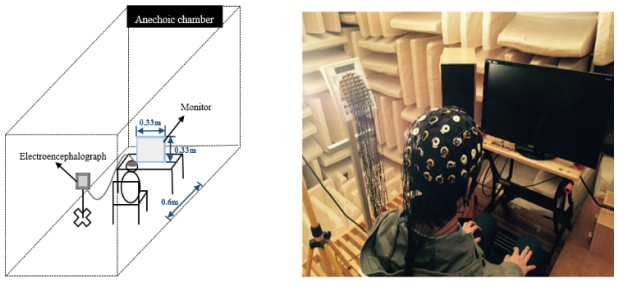

FIGURE 5. Experimental setup.

equipment, the experiment was conducted in an anechoic chamber. Moreover, during the experiment, no other lights could reach the LCD.

B. COMPARISON OF PRESENTATION MODE

The pattern-reversal checkerboard, an effective strategy to stimulate the brain's visual neurons, can always be used for the SSVEP experiment. For eliciting a possible strong SSVEP response, three types of presentation modes were examined: full-screen (resembling a blinking LED), 2 × 2 checkerboard, and 4 × 4 checkerboard (Figure 6). These modes were enables by presenting a stimulus at the frequency of 12 Hz, which elicits a strong response [17].

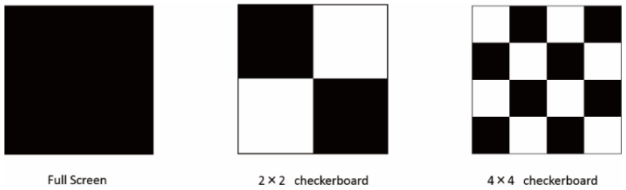

FIGURE 6. Presentation mode of stimulus. Full-screen (left), 2 × 2 checkerboard (middle), and 4 × 4 checkerboard (right).

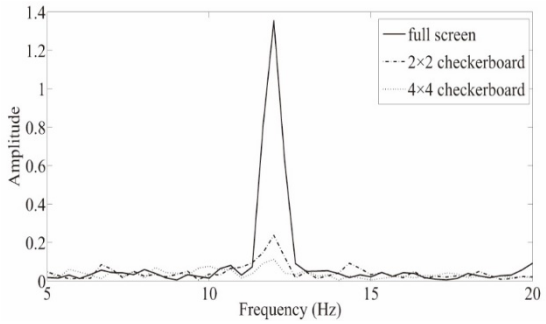

FIGURE 7. FFT analysis of EEG data following presentation of stimuli at 12 Hz.

Each stimulus was presented for 3 s, the synchronous addition was performed 30 times, and each stimulus was followed by a 3-s rest interval. EEG measurements were obtained while participants gazed at the center of the screen.

Figure 7 depicts the analysis results of EEG data following presentation of stimuli at 12 Hz using FFT. With respect to the amplitude value of 12 Hz, the full-screen stimulus was the highest, resulting in the strongest SSVEP response. In contrast, responses to both checkerboard patterns were weak, although the response to the 4 × 4 pattern was weaker than that to the 2 × 2 pattern. Therefore, full-screen stimuli were used in the present study.

TABLE 1. Stimulus presentation.

Frequency of stimulus	Time of stimulus	Rate of stimulus
6-15 Hz	1 second, 2 seconds, 3 seconds	9 Hz/s, 4.5 Hz/s, 3 Hz/s
12-33 Hz	7 seconds	3 Hz/s
8-48 Hz	5 seconds	8 Hz/s

C. SELECTION OF STIMULUS

To measure differences in responses to each band, the following types of stimuli with a sampling frequency of 2000 Hz were presented (Table 1):

1. For measuring the response of α band of 7-13 Hz and examining the influence of the inclination of the chirp stimulus frequency variation, the frequency of the stimulus changes from 6-15 Hz over a duration of 1, 2, and 3 s were prepared; thus, the stimulus at rates of 9, 4.5, and 3 Hz/s, respectively.
2. For measuring the response of β band of 13-30 Hz and unifying the inclination of frequency variation with the last stimulus at 3 Hz/s, the frequency of the stimulus that changed from 12 to 33 Hz over 7 s was prepared.
3. For determining the band in which the stronger response occurred, a wide frequency band of the stimulus which contained both the α and β bands was selected. As a broadband stimulus requires a long presentation period, the frequency of the stimulus that changed from 8 to 48 Hz over 5 s was prepared, and the rate of this stimulus was 8 Hz/s.

Each task was performed 50 times, with a rest interval of 3 s between each task.

IV. RESULTS OF STFT ANALYSIS AND NHA FOR EACH STIMULUS

Shortening the analysis window should theoretically emphasize the SSVEP, because NHA can maintain a high frequency resolution even when a short time window is used since the length of the analysis window exerts little influence. Therefore, we selected an analysis window length of 500 (0.25 s) for NHA. However, because of the poor frequency resolution of STFT and its comparatively greater dependence on the length of the analysis window, it cannot be used to analyze stimuli within a short time window. Thus, an analysis window length of 1,000 (0.5 s) was selected for STFT, for which the Hamming window was also utilized.

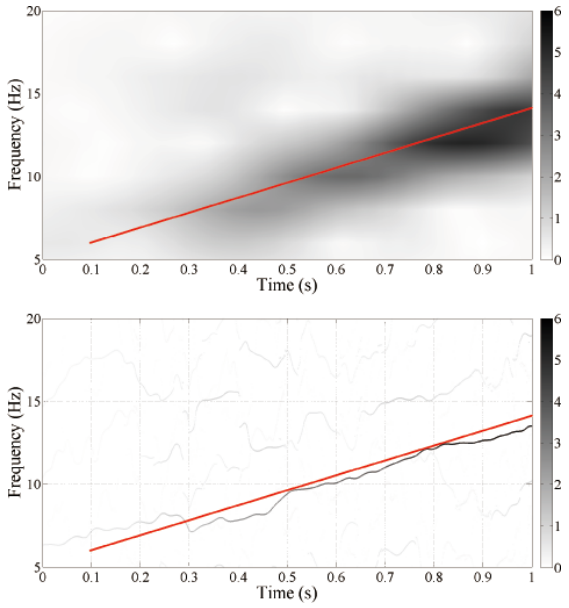

FIGURE 8. Results of STFT analysis (up) and NHA (down) for stimuli whose frequency changed from 6-15 Hz over 1 s under window lengths of 1,000 (0.5 s) and 500 (0.25 s), respectively. The red line indicates the frequency of stimulus presentation.

The results of analysis for each band using the STFT and NHA are shown in Figures 8-12, and the red line of each figure indicates the frequency of stimulus presentation with a sampling frequency of 2000 Hz.

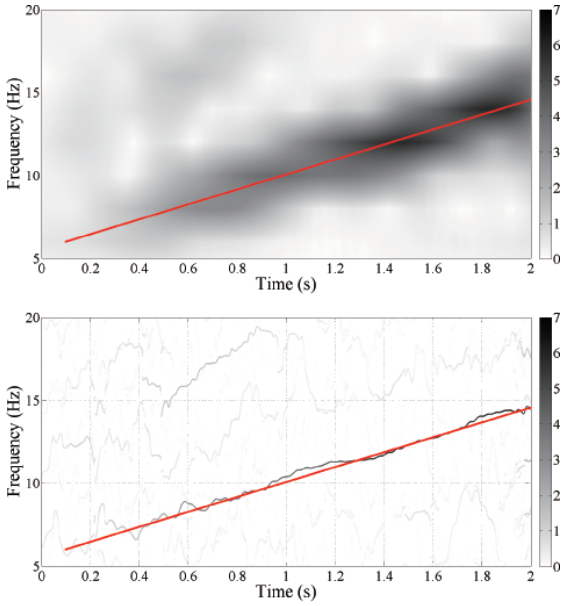

FIGURE 9. Results of STFT analysis (up) and NHA (down) for stimuli whose frequency changed from 6-15 Hz over 2 s under window lengths of 1,000 (0.5 s) and 500 (0.25 s), respectively. The red line indicates the frequency of stimulus presentation.

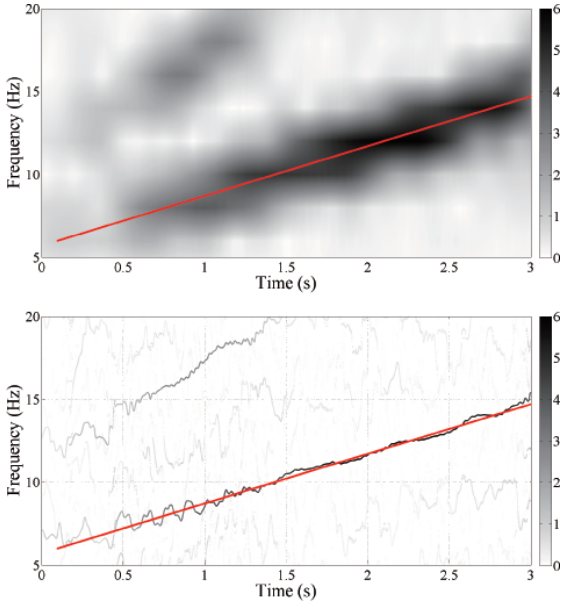

FIGURE 10. Results of STFT analysis (up) and NHA (down) for stimuli whose frequency changed from 6-15 Hz over 3 s under window lengths of 1,000 (0.5 s) and 500 (0.25 s), respectively. The red line indicates the frequency of stimulus presentation.

Figures 8-10 present the results of EEG analysis for stimuli presented at 6-15 Hz, which included the α band over 1, 2, and 3 s.

Figure 8 shows that STFT could not perceive the response as the influence of the analysis window is large and the frequency of the stimulus changed rapidly. In addition, substantially severe distortion was observed over a large area, especially for strong responses under 15 Hz. In the case of NHA, as the length of the analysis window exerted little influence, no side-lobe artifacts were observed, the frequency change of the response was visualized as a line, allowing for a clear and easy capture of the response even if the frequency variation of the stimulus is large.

In accordance with the findings of previous studies, Figure 9 shows that the amplitude of the SSVEP is the highest at a frequency of approximately 12 Hz [21], [48]. Our results indicated that because of the low-frequency resolution of STFT analyses, it could only produce section-by-section views of the frequency change and the responses were blurred severely. However, NHA enabled the visualization of the stimulus as a continuous line and the area surrounding the response remained clear because of the high frequency resolution.

The results presented in Figure 10 are nearly identical to those in Figure 9, except that the reaction of the overtone component has become stronger.

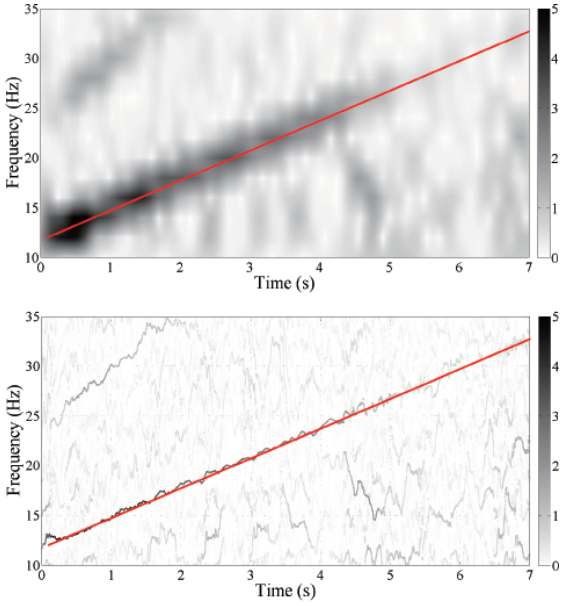

FIGURE 11. Results of STFT analysis (up) and NHA (down) for stimuli whose frequency changed from 12-33 Hz over 7 s under window lengths of 1,000 (0.5 s) and 500 (0.25 s), respectively. The red line indicates the frequency of stimulus presentation.

Figure 11 depicts the results of EEG analysis for stimuli presented at 12-33 Hz, which includes the β band. The highest amplitude values can be observed at 12 Hz. An examination of the overtone component demonstrated that the amplitude values were the same as those observed for the basic frequency within the same frequency band. These findings indicate that the amplitude of the overtone component depends on the frequency band.

Figure 12 presents the results of EEG analysis for stimuli presented at 8-48 Hz, which includes both the α and β bands. As observed for stimuli presented at 6-15 Hz, the highest amplitude values can be observed at a frequency of approximately 12 Hz, and increases in frequency were

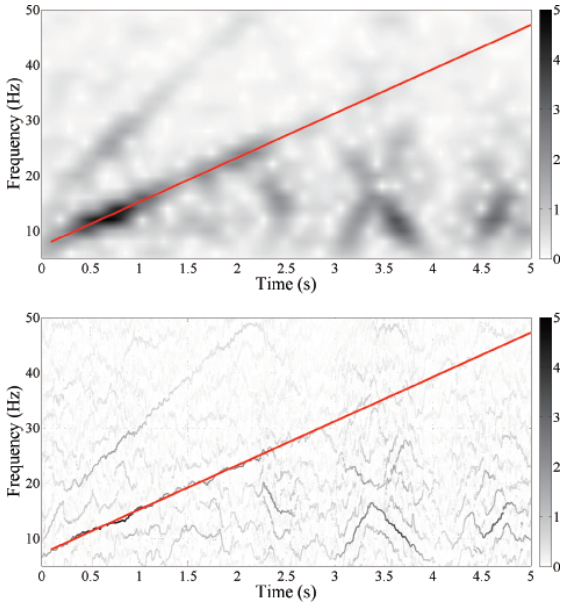

FIGURE 12. Results of STFT analysis (up) and NHA (down) for stimuli whose frequency changed from 8-48 Hz over 5 s under window lengths of 1,000 (0.5 s) and 500 (0.25 s), respectively. The red line indicates the frequency of stimulus presentation.

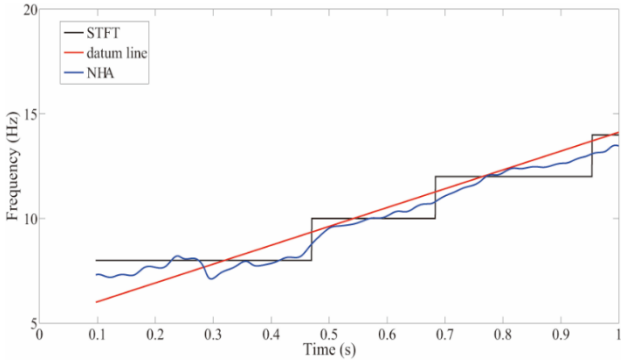

FIGURE 13. Spectra estimated of stimuli whose frequency changed from 6-15 Hz over 1 s using the STFT, NHA, and datum line.

accompanied by decreases in amplitude. Amplitude values were particularly low above 30 Hz, and responses were difficult to determine for frequencies higher than 40 Hz.

V. DISCUSSION

For stimuli whose frequency changed from 6-15 Hz over 1 s, the frequency started from 6 Hz at about 0.1 s and reached 14 Hz at approximately 1 s, as shown in Figure 8. Therefore, a frequency component with the maximum amplitude of STFT and NHA results was extracted at each time point in the 0.9 s period from 0.1 s to 1 s. In addition, the frequency of stimulus presentation in the same time period was extracted and used as the datum line. Figure 13 shows the STFT, NHA, and the datum line extraction results in the same 0.9 s period from 0.1 s to 1 s, and the characteristic of frequency change of STFT was step-wise due to its low time-frequency resolution.

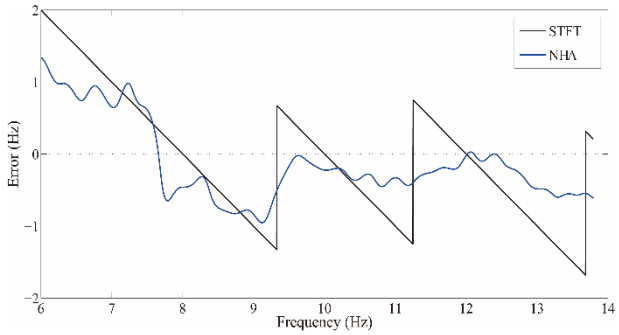

FIGURE 14. Frequency errors of the STFT and NHA results from 6-14 Hz.

The frequency errors of the STFT and NHA results were calculated by:

$$e = \sqrt{\frac{\sum_{m=1}^{M}\left[f\ (m) - \hat{f}(m)\right]^2}{M}} \tag{11}$$

where e is the mean frequency error of the extracted interval of the STFT or NHA results and the datum line; M is the number of STFT, NHA, and datum line data in the extracted interval; $f(\mathrm{m})$ is the STFT or NHA data in the extracted interval; and $\hat{f}(\mathrm{m})$ is the datum line data in the extracted interval.

In the case of STFT, the mean frequency error of this interval was 1.2646 Hz. However, the mean frequency error in the NHA case was 0.4361 Hz, which is almost a third of the STFT error.

Moreover, the standard deviation of STFT and NHA errors were also calculated. The standard deviation was 2.6601Hz for STFT, and NHA was 1.3402 Hz, which is almost half of the STFT indicates that NHA had a low degree of dispersion.

Figure 14 presents the frequency errors of the STFT and NHA results from 6-14 Hz. It was distinct that NHA had a much smaller error than STFT. And from 6-9 Hz, the error was higher than 9-14 Hz in the NHA case. Although STFT had basically similar trend, the margin of error was much larger, especially at each turning point. Thus, the analytical precision of NHA was quite high, even with significant noise.

In the same way, the mean frequency errors and standard deviations of the rest of the stimuli were calculated and are listed in Table 2.

For the stimulus of 12-33 Hz over 7 s and 8-48 Hz over 5 s, the mean frequency errors and standard deviations of both methods were large since the response disappeared after half the time of each stimulus, and the error was calculated to the end time of each stimulus. However, the mean frequency errors and standard deviations of NHA were still at least half the magnitude of the STFT errors.

Consequently, the validity of NHA is very high, and that it enables accurate estimation and detailed analysis, captures changes in the angle of the frequency correctly, and is appropriate for use in LCD-based experiments.

TABLE 2. Mean frequency error and standard deviation of each stimulus using STFT and NHA.

Frequency of stimulus	Extracted time period	Mean frequency error (STFT)	Mean frequency error (NHA)	Standard deviation (STFT)	Standard deviation (NHA)
6-15 Hz (1 s)	0.1-1 second	1.2646 Hz	0.4361 Hz	2.6601 Hz	1.3402 Hz
6-15 Hz (2 s)	0.1-2 seconds	1.2851 Hz	0.5379 Hz	2.8140 Hz	1.4691 Hz
6-15 Hz (3 s)	0.1-3 seconds	2.0742 Hz	0.8059 Hz	3.1612 Hz	1.8423 Hz
12-33 Hz (7 s)	0.1-7 seconds	8.5069 Hz	3.7255 Hz	5.3951 Hz	2.3357 Hz
8-48 Hz (5 s)	0.1-5 seconds	19.5780 Hz	9.8521 Hz	7.9786 Hz	3.9533 Hz

In conclusion, NHA is effective for obtaining accurate spectral representations of stimulus, and NHA affords high time frequency resolution, analytical precision, and noise reduction.

VI. CONCLUSION

With the popularity of the IoT, which plays an irreplaceable and important role in the field of medical processing. And in the present study, we evaluated EEG responses when a chirp stimulus was presented on an LCD monitor to participants. Our findings indicated that the use of grayscale images reduces the frequency distortion associated with the refresh rate of the monitor as the stimulus is presented as a sinusoidal pattern.

Our results further indicated that STFT analyses are dependent on the length of the analysis window. Although the length of the analysis window for STFT is twice as long as that for NHA, STFT analysis still produces section-by-section views of the frequency change and exhibits low frequency resolution. Moreover, STFT enables only a rough trace when the frequency of the stimulus changes because only the phased value of the frequency can be expressed and visualized. The line is thick and blurred due to the presence of the large main-lobe and side-lobe artifacts, which indicate poor reproducibility for LCD monitors. SSVEPs were difficult to perceive using STFT analyses, so it was difficult to perform a detailed analysis and observe the response change.

In contrast, the frequency changes that could not be analyzed by STFT analyses can be analyzed and visualized using NHA. Since NHA can overcome the influence of the analysis window and suppresses the side-lobe artifacts efficiently, it allows for an accurate assessment of the frequency values and other associated parameters. Furthermore, NHA enabled the measurement of Chirp-VEPs—which could be visualized as a continuous line and used to clearly capture even faint signals—using a short time window; thus, it is possible to observe and analyze the response in great detail. Moreover, the results of NHA were highly similar and often overlapped the datum line representing the frequency of the stimulus presentation (red line). The mean frequency errors and standard deviations were distinctly less than those for STFT.

Our results indicate that NHA is effective for analyzing Chirp-VEPs and changes in brain waves, suggesting that NHA is a highly precise analysis method that can be used to simultaneously achieve high frequency resolution and time resolution. We will attempt to analyze responses to more colorful stimuli on an LCD monitor using NHA without preprocessing in future experimental environments.

ACKNOWLEDGMENT

The authors would like to thank all collaborators for their time and all reviewers for their valuable suggestions.

REFERENCES

[1] Linux.com. *Who Needs the Internet of Things?* Accessed: Nov. 16, 2018. [Online]. Available: https://www.linux.com/news/who-needs-internet-things

[2] C.-M. Huang, Y.-F. Chen, S. Xu, and H. Zhou, "The vehicular social network (VSN)-based sharing of downloaded geo data using the credit-based clustering scheme," *IEEE Access*, vol. 6, pp. 58254–58271, 2018.

[3] H. Zhou, H. Wang, X. Chen, X. Li, and S. Xu, "Data offloading techniques through vehicular ad hoc networks: A survey," *IEEE Access*, vol. 6, pp. 65250–65259, 2018.

[4] H. Zhang, Y. Qi, H. Zhou, J. Zhang, and J. Sun, "Testing and defending methods against DoS attack in state estimation," *Asian J. Control.*, vol. 19, no. 3, pp. 1295–1305, 2017.

[5] C. Zhu, V. C. M. Leung, J. J. P. C. Rodrigues, L. Shu, L. Wang, and H. Zhou, "Social sensor cloud: Framework, greenness, issues, and outlook," *IEEE Netw.*, vol. 32, no. 5, pp. 100–105, Sep./Oct. 2018.

[6] G. J. Joyia, R. M. Liaqat, A. Farooq, and S. Rehman, "Internet of medical things (IOMT): Applications, benefits and future challenges in healthcare domain," *J. Commun.*, vol. 12, no. 4, pp. 240–247, 2017.

[7] R. Xu, N. Jiang, C. Lin, N. Mrachacz-Kersting, K. Dremstrup, and D. Farina, "Enhanced low-latency detection of motor intention from EEG for closed-loop brain-computer interface application," *IEEE Trans. Biomed. Eng.*, vol. 61, no. 2, pp. 288–296, Feb. 2014.

[8] J. Kevric and A. Subasi, "Comparison of signal decomposition methods in classification of EEG signals for motor-imagery BCI system," *Biomed. Signal Process. Control*, vol. 31, pp. 398–406, Jan. 2017.

[9] S. A. Sprague, M. T. McBee, and E. W. Sellers, "The effects of working memory on brain–computer interface performance," *Clin. Neurophysiol.*, vol. 127, pp. 1331–1341, Feb. 2016.

[10] S. P. Levine *et al.*, "A direct brain interface based on event-related potentials," *IEEE Trans. Rehabil. Eng.*, vol. 8, no. 2, pp. 180–185, Jun. 2000.

[11] L. Piccini, S. Parini, L. Maggi, and G. Andreoni, "A wearable home BCI system: Preliminary results with SSVEP protocol," in *Proc. IEEE 27th Annu. Int. Conf. Eng. Med. Biol. Soc.*, Jan. 2006, pp. 5384–5387.

[12] J. Ando, J. Toyama, H. Shigemasu, N. Matsuzaki, and M. Kitazaki, "Quantitative steering of a driving simulator by steady-state visual evoked potentials," *Trans. Virtual Reality Soc. Jpn.*, vol. 15, no. 1, pp. 33–40, 2010.

[13] H. Bakardjian, T. Tanaka, and A. Cichocki, "Optimization of SSVEP brain responses with application to eight-command brain-computer interface," *Neurosci. Lett.*, vol. 469, pp. 34–38, Jan. 2010.

[14] G. Rodríguez-Bermúdez, P. J. García-Laencina, J. Roca-González, and J. Roca-Dorda, "Efficient feature selection and linear discrimination of EEG signals," *Neurocomputing*, vol. 115, pp. 161–165, Sep. 2013.

[15] J. Atkinson and D. Campos, "Improving BCI-based emotion recognition by combining EEG feature selection and kernel classifiers," *Expert Syst. Appl.*, vol. 47, pp. 35–41, Apr. 2016.
[16] M. Sengelmann, A. K. Engel, and A. Maye, "Maximizing information transfer in SSVEP-based brain–computer interfaces," *IEEE Trans. Biomed. Eng.*, vol. 64, no. 2, pp. 381–394, Feb. 2017.
[17] W. Yijun, W. Ruiping, G. Xiaorong, and G. Shangkai, "Brain-computer interface based on the high-frequency steady-state visual evoked potential," in *Proc. IEEE Neural Interface Control*, May 2005, pp. 37–39.
[18] P. Poryzala, M. Byczuk, and A. Materka, "A virtual keypad based on alternate half-field stimulated visual evoked potentials," in *Proc. Int. Symp. Inf. Technol. Converg.*, 2007, pp. 296–300.
[19] T. Sakurada, T. Kawase, T. Komatsu, and K. Kansaku, "Use of high-frequency visual stimuli above the critical flicker frequency in a SSVEP-based BMI," *Clin. Neurophysiol.*, vol. 126, pp. 1972–1978, Oct. 2015.
[20] H.-J. Hwang, J.-H. Lim, Y.-J. Jung, H. Choi, S. W. Lee, and C.-H. Im, "Development of an SSVEP-based BCI spelling system adopting a QWERTY-style LED keyboard," *J. Neurosci. Methods*, vol. 208, no. 1, pp. 59–65, Jun. 2012.
[21] E. Sheppard *et al.*, "Children with a history of atypical febrile seizures show abnormal steady state visual evoked potential brain responses," *Epilepsy Behav.*, vol. 27, pp. 90–94, Apr. 2013.
[22] T. Tu, Y. Xin, X. Gao, and S. Gao, "Chirp-modulated visual evoked potential as a generalization of steady state visual evoked potential," *J. Neural Eng.*, vol. 9, p. 016008, Dec. 2012.
[23] A. M. Dreyer and C. S. Herrmann, "Frequency-modulated steady-state visual evoked potentials: A new stimulation method for brain–computer interfaces," *J. Neurosci. Meth.*, vol. 241, pp. 1–9, Feb. 2015.
[24] J. Artieda, M. Valencia, M. Alegre, O. Olaziregi, E. Urrestarazu, and J. Iriarte, "Potentials evoked by chirp-modulated tones: A new technique to evaluate oscillatory activity in the auditory pathway," *Clin. Neurophysiol.*, vol. 115, pp. 699–709, Mar. 2004.
[25] R. Kuś *et al.*, "On the quantification of SSVEP frequency responses in human EEG in realistic BCI conditions," *PLoS ONE*, vol. 8, no. 10, p. e77536, 2013.
[26] H. Shen, L. Zhao, Y. Bian, and L. Xiao, "Research on SSVEP-based controlling system of multi-DoF manipulator," in *Proc. Int. Symp. Neural Netw.*, 2009, pp. 171–177.
[27] Z. İşcan and V. V. Nikulin, "Steady state visual evoked potential (SSVEP) based brain-computer interface (BCI) performance under different perturbations," *PLoS ONE*, vol. 13, no. 1, p. e0191673, 2018.
[28] T. Yoshizawa, S. Hirobayashi, and T. Misawa, "Noise reduction for periodic signals using high-resolution frequency analysis," *EURASIP J. Audio Speech Music Process.*, vol. 2011, no. 5, 2011.
[29] M. Hasegawa, T. Kako, S. Hirobayashi, T. Misawa, T. Yoshizawa, and Y. Inazumi, "Image inpainting on the basis of spectral structure from 2-D nonharmonic analysis," *IEEE Trans. Image Process*, vol. 22, no. 8, pp. 3008–3017, Aug. 2013.
[30] F. Hosotani, Y. Inuzuka, M. Hasegawa, S. Hirobayashi, and T. Misawa, "Image denoising with edge-preserving and segmentation based on mask NHA," *IEEE Trans. Image Process*, vol. 24, no. 12, pp. 6025–6033, Dec. 2015.
[31] T. Ueda, K. Fujii, S. Hirobayashi, T. Yoshizawa, and T. Misawa, "Motion analysis using 3D high-resolution frequency analysis," *IEEE Trans. Image Process.*, vol. 22, no. 8, pp. 2946–2959, Aug. 2013.
[32] T. Ichinose, S. Hirobayashi, T. Misawa, and T. Yoshizawa, "Forecast of stock market based on nonharmonic analysis used on NASDAQ since 1985," *Appl. Financial Econ.*, vol. 22, no. 3, pp. 197–208, 2012.
[33] D. Jia *et al.*, "Multiwindow nonharmonic analysis method for gravitational waves," *IEEE Access*, vol. 6, pp. 48645–48655, 2018.
[34] D. Jia *et al.*, "Time–frequency-based non-harmonic analysis to reduce line-noise impact for LIGO observation system," *Astron. Comput.*, vol. 25, pp. 238–246, Oct. 2018.
[35] T. Uchida *et al.*, "Non-uniform non-harmonic analysis method development and verification of applicability to swept source optical coherence tomography," *Nonlinear Theory Appl.*, vol. 4, no. 2, pp. 172–182, 2013.
[36] X. Cao *et al.*, "Non-harmonic analysis applied to optical coherence tomography imaging," *Jpn J. Appl. Phys.*, vol. 51, p. 022503, Feb. 2012.
[37] T. Uchida, Y. Inuzuka, M. Hasegawa, S. Hirobayashi, and T. Misawa, "Numerical simulation validation of nonuniform, nonharmonic analysis of spectral-domain optical coherence tomography," *Opt. Eng.*, vol. 54, no. 3, p. 033108, 2015.
[38] B. Allison, D. McFarland, G. Schalk, S. Zheng, M. Jackson, and J. Wolpaw, "Towards an independent brain-computer interface using steady state visual evoked potentials," *Clin. Neurophysiol.*, vol. 119, no. 2, pp. 399–408, 2008.
[39] M. Nakanishi, Y. Wang, Y. T. Wang, Y. Mitsukura, and T.-P. Jung, "Generating visual flickers for eliciting robust steady-state visual evoked potentials at flexible frequencies using monitor refresh rate," *PLoS ONE*, vol. 9, no. 6, p. e99235, 2014.
[40] I. Y. Soon and S. N. Koh, "Speech enhancement using 2-D Fourier transform," *IEEE Trans. Speech Audio Process.*, vol. 11, no. 6, pp. 717–724, Nov. 2003.
[41] S. Hirobayashi, F. Ito, T. Yoshizawa, and T. Yamabuchi, "Estimation of the frequency of non-stationary signals by the steepest descent method," in *Proc. 4th Asia–Pacific Conf. Ind. Eng. Manage. Syst.*, 2002, pp. 788–791.
[42] J. W. Tukey and A. E. Beaton, "The fitting of power series, meaning polynomials, illustrated on band-spectroscopic data," *Technometrics*, vol. 16, no. 2, pp. 147–185, 1974.
[43] J. M. Chambers, *Computational Methods for Data Analysis*. New York, NY, USA: Wiley, 1977.
[44] P. E. Gill and W. Murray, "Quasi-Newton methods for unconstrained optimization," *IMA J. Appl. Math.*, vol. 9, no. 1, pp. 91–108, Feb. 1972.
[45] E. B. George and M. J. T. Smith, "Speech analysis/synthesis and modification using an analysis-by-synthesis/overlap-add sinusoidal model," *IEEE Trans. Speech Audio Process.*, vol. 5, no. 5, pp. 389–406, Sep. 1997.
[46] E. B. George and M. J. T. Smith, "Analysis-by-synthesis/overlap add sinusoidal modeling applied to the analysis and synthesis of musical tones," *J. Audio Eng. Soc.*, vol. 40, no. 6, pp. 497–516, 1992.
[47] Ethics Committee, University of Toyama. *Ethical Review of Research for Non-Medical Purposes*. Accessed: Nov. 29, 2018. [Online]. Available: http://www.hosp.u-toyama.ac.jp/tiken/cec/EthicsCommittee-gohuku.html
[48] G. Garcia, "High frequency SSVEPs for BCI applications," in *Proc. Brain-Comput. Interfaces HCI Games Workshop*, Florence, Italy, 2008.

DONGBAO JIA received the M.E. and Ph.D. degrees from the Department of Intellectual Information Engineering, Graduate School of Science and Engineering for Education, University of Toyama, Toyama, Japan, in 2015 and 2018, respectively, where he is also a Special Researcher. He is currently a Lecturer with the School of Computer Engineering, Huaihai Institute of Technology, Lianyungang, China. His main research interests include signal processing, time–frequency analysis, and neural engineering.

HONGWEI DAI received the B.S. and M.S. degrees from Xi'an Jiaotong University, Shaanxi, China, in 1999 and 2002, respectively, and the D.E. degree, in 2007. From 2002 to 2003, he was a Lecturer with the Institute of Mechatronics and Information System, Xi'an Jiaotong University. In 2008, he joined the Huaihai Institute of Technology, Jiangsu, China, where he is currently the Vice Dean and an Associate Professor with the School of Computer and Engineering. From 2013 to 2014, he was an Academic Visitor with the Control System Center, The University of Manchester. His current research interests include computational intelligence, pattern recognition, complex networks, and optimizations.

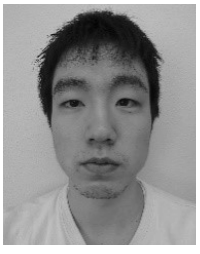

YUTA TAKASHIMA received the B.E. degree in intellectual information engineering from the University of Toyama, Toyama, Japan, in 2016, where he is currently pursuing the degree with the Department of Intellectual Information Engineering, Graduate School of Science and Engineering for Education. His research interest includes signal processing.

TAKURO NISHIO is currently pursuing the degree with the Department of Intellectual Information Engineering, University of Toyama. His research interest includes neural engineering.

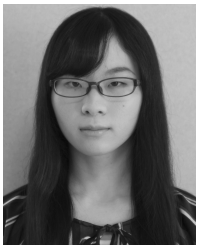

KANNA HIROBAYASHI is currently pursuing the degree with the Department of Intellectual Information Engineering, University of Toyama. Her research interests include signal processing and NMR imaging.

MASAYA HASEGAWA received the B.E., M.E., and Ph.D. degrees from the University of Toyama, in 2012, 2014, and 2017, respectively, and the D.Eng. degree from the University of Toyama, where he is currently a Research Assistant Professor. His research interests include multidimensional signal analysis, high-accuracy analysis, image processing, and medical image analysis.

SHIGEKI HIROBAYASHI received the D.Eng. degree from the University of Toyama, where he is currently a Professor. He has been involved in acoustic signal processing, acoustic field control, and image processing. He is a member of the Institute of Electronics Information and Communication Engineers, the Institute of Electrical Engineers of Japan, the Acoustic Society of Japan, the Acoustic Society of America, and the IEEE.

TADANOBU MISAWA received the B.E., M.E., and Ph.D. degrees from Kanazawa University, in 1999, 2001, and 2004, respectively. He was a Doctoral Fellow with the Kanazawa Institute of Technology, in 2004. He was an Assistant Professor with the School of Management, Tokyo University of Science, in 2005. He is currently an Associate Professor with the Graduate School of Science and Engineering, University of Toyama. His research interests include artificial intelligence and brain–computer interfaces.